Wavelength stabilization in an excimer laser source using piezoelectric active vibration control

Ronald Spangler*, Robert Jacques, Active Control eXperts, Inc.
Daniel Brown†, J. Martin Algots, William Partlo, Cymer, Inc.

ABSTRACT

Excimer laser light sources for photolithography are subject to a cycle of ever-tightening precision requirements, dictated by the design-rule shrinks planned into the industry roadmap. But pulse-to-pulse stability of the center wavelength of the emitted light is limited by the presence of vibration in key components and structures. This paper covers the application of Active Vibration Control (AVC) technology to an excimer laser to mitigate the effects unwanted vibration, and enable compliance with anticipated future stability specifications. The laser system is described, from a structural-dynamics point of view. A systematic approach to vibration diagnostics is presented, with experimental results to support key conclusions regarding the types and sources of vibrations. Next, analytical assessment of active control performance is discussed, followed by breadboard-type implementation results showing reductions of >30% in a key stability performance metric.

Keywords: Control, lithography, vibration, excimer, laser, servo, piezoelectric

1. INTRODUCTION

To help semiconductor manufacturers keep pace with Moore's Law, OEMs of precision manufacturing equipment must continue to grapple with aggressive accuracy, stability and throughput requirements. The error budget for these requirements is affected by a variety of variables, including vibration. At each level of innovation and complexity, controlling vibration becomes increasingly important. Today, designers not only must isolate machines from external vibrations, but must also focus on the more challenging, internally generated disturbances. Traditional methods of vibration mitigation may prove inadequate to the task of controlling the effects of these disturbances. Similarly, traditional methods of servo control will experience limitations due to structural and other mechanical vibrations which have not to date been problematic. A new type of systems-level design is needed to create servo-elastic control systems which achieve the required combination of throughput and precision demanded by the industry. Additional tools, including Active Vibration Control (AVC), will be needed to work in conjunction with existing methods, to create this new type of high-performance servo-elastic control system.

The excimer lasers used in semiconductor processing are subject to similarly tightening requirements, in this case on the parameters of the emitted pulse stream. Design-rule shrinks are driving photolithography toolmakers toward optics with larger numerical aperture (NA), requiring tightening of the laser spectral bandwidth to allow sufficient depth-of-focus control. The center-wavelength of the laser spectrum must also exhibit increased stability over time, to enable the use of these smaller depth-of-focus optics. Pulse to pulse energy dose instability also impacts CD control, although increasing repetition rate, thereby increasing the number of pulses in the exposure window, can help stabilize the total dosage. However, increasing throughput requirements on the stepper/scanner will drive the number of pulses per window back downward. In general, the tightening of spectral bandwidth, and the increased stability requirement on the pulse center wavelength, must be achieved in spite of, and not with the help of, the increase in pulse repetition rates needed to maximize throughput in the fab. Driven by both increasing throughput and increasing accuracy requirements, manufacturers such as Cymer have in the past four years delivered a fourfold increase in pulse repetition rates, while simultaneously reducing the spectral bandwidth by half.

Control of both the spectral bandwidth and the center wavelength of excimer laser light is achieved by directing the beam onto a dispersive optical element at a precise angle. To meet future requirements, both the precision of control of the incident angle, as well as stability of this angle about its mean, will place severe requirements on the stability of the structures and mechanisms which support and position the relevant optics. Uncontrolled motion of anything in the light-path may limit the achievable beam steering precision, and therefore the achievable accuracy and stability of the center wavelength.

* rocket@acx.com; phone 617.577.0700 x246; http://www.acx.com; ACX, Inc., 215 First St., Cambridge, MA 02142
† dbrown@cymer.com; phone 858.385.5270; http://www.cymer.com; Cymer, Inc., 16750 Via Del Campo Ct., San Diego, CA 92127

Vibration is an unavoidable aspect of the operating environment of precision machinery. No structure or mechanism can be made infinitely rigid; no onboard moving part can be made perfectly smooth and quiet; and Newton's third law cannot be repealed, so motion (acceleration) will always necessarily induce inertial reaction forces into a structure. When requirements on precision shrink to the point at which vibration becomes the limiting factor, machine designers have traditionally made use of a set of tools, including

- Stiffening the key structures and mechanisms, to move resonant frequencies out of the bandwidth of concern. As the bandwidth of disturbances increases into the kHz range and beyond, it becomes more and more difficult to push all resonances (modes of vibration) out of reach.
- Passive damping, to reduce the response level of problem modes. Passive damping is traditionally achieved through inertial methods, such as tuned-mass dampers, through strain-based methods such as constrained-layer viscoelastic treatments, or through other less widely-used methods such as frictional dampers. These methods are somewhat limited in performance, for various reasons and in various regimes, and can suffer other drawbacks such as outgassing, temperature dependence, and generation of particulates which can obscure key optical elements or otherwise violate clean room protocols.
- Isolation of the disturbance sources from the rest of the machine. First, various passive techniques exist to isolate a machine from vibrational energy transmitted through the floor. But these techniques are not effective for disturbance sources, such as fans or moving stages, onboard the machine. In certain cases these onboard disturbances can be isolated from the rest of the machine using rubber mounts (or other polymeric materials), but material sag and creep tends to work against the static alignment requirements often present in such machinery, especially when such requirements are stated in nanometers.

In this paper, we present a novel alternative to the traditional approaches, based on active vibration control (AVC). The elements of the AVC system, including vibration sensors, digital feedback algorithms, and control actuation are discussed. Results are presented showing improved wavelength stability with active control vs. the uncontrolled system.

2. LASER SYSTEM DESCRIPTION

This study was conducted on a modified Cymer ELS-6000 excimer laser. The ELS-6000 is a KrF laser which emits deep UV light pulses at a nominal 248 nm wavelength. Other specifications and typical wavelength stability requirements are listed in Table 1.

Table 1: ELS-6000 Specifications and Typical Wavelength Stability Requirements

Parameter	Specification/ Requirement	Range Tested
Wavelength	248 nm	248 nm
Repetition Rate Max	2000 Hz	1000—2500 Hz
Pulse Energy	10 mJ	7.5 mJ
Moving Window Size	30 pulses	--
Moving Average Wavelength Error	-0.05 pm $< MA\lambda < 0.05$ pm	--
Moving Standard Deviation Error	$MSD\lambda < 0.05$ pm	--

The light pulses are created via a high-voltage electrical discharge in the gas-filled chamber. This discharge happens at repetition rates up to 2000 Hz in the ELS-6000, though the testbed used in this study was run at rates up to 2500 Hz for characterization purposes. (To achieve this higher rate while maintaining average output power at 20W, the pulse energy was limited to 75% of rated maximum.) The electrical discharge is known to create acoustic pressure waves in the gas-filled chamber. These pressure waves will impact with the chamber walls, and can excite mechanical resonances elsewhere in the system. In the frequency domain, the discharge disturbance energy spectrum will possess narrowband components at $N*f_R$, where f_R is the repetition rate, and $N = 1, 2, 3, \ldots$.

The gas in the chamber is circulated via a large cylindrical ("squirrel cage") fan, to refresh the gas in the region of the discharge electrodes between pulses. This fan is another source of acoustic and mechanical disturbance energy, through its blade-passage interaction with the gas, and through mounting via bearings to the chamber, and thereby to the rest of the laser frame structure.

The laser cavity is formed by mounting (partially) reflective optics on either side of the chamber. Wavelength and bandwidth control are achieved in the Line Narrowing Module, on the left side of the chamber. In this module, the light beam is spread by a series of prisms, and directed onto an articulated tilt mirror. This steering mirror then reflects the beam onto a dispersive grating which retro-reflects only a narrow spectral band, scattering all other frequencies. Thus line narrowing is achieved passively via the grating, while the center wavelength of the narrowed spectrum is dictated (in a narrow range about the nominal value) by the angle of incidence onto the grating. On the other side of the laser cavity, a portion of the exiting beam is split off into the Stabilization Module, in which the pulse energy, bandwidth, and center wavelength are measured for each pulse.

Selecting wavelength involves positioning the steering mirror to a precise angle, which is done on the production ELS-6000 using a mechanism including a stepper motor, reduction gears, and a reduction lever arm. The mirror is closed-loop controlled via a servo using the wavelength measurements. Servo control involves using feedback to drive the error between a desired position or trajectory to as close to zero as possible as fast as possible. The accuracy and speed of a servo-controlled system are generally limited by the precision and response time of the sensor and actuator components. The ELS-6000 meets its wavelength stability specifications with a good margin of safety, but the stepper motor is neither fast nor precise enough to allow the wavelength servo to perform to expected specifications on future lasers. To address these future needs, Cymer has developed a new LNM with a second stage of finer/faster steering mirror actuation using a piezoelectric PZT stack actuator. A prototype of this new LNM was used in the current study.

Anything in the light path which affects the angular alignment of the laser beam will cause some wavelength error. "Anything" includes acoustic pressure waves in the chamber, or unwanted motion of key optical components and the associated support structures. Wavelength error is quantified by two key metrics, moving-window average (MAλ) and moving-window standard deviation (MSDλ). MAλ is in effect a recursive digital lowpass filter, and therefore will be sensitive to relatively long time-scale errors such as that induced by thermal drift. MSDλ is conversely sensitive to the fast variation or jitter associated with mechanical and acoustic vibrations. MAλ errors can impact depth of focus. MSDλ errors, when integrated over a typical exposure window, can widen the effective spectral bandwidth, causing increased chromatic aberrations errors on the wafer.

3. DIAGNOSTIC BASELINE TESTING

Determining the impact, if any, of vibration on the performance of a typical excimer laser involved applying a three-step diagnostic process to the ELS-6000 testbed. Step one involves quantifying the vibrational contribution to the key performance metrics, MAλ and MSDλ. Step two involves identifying the physical sources of excitation for these vibrations. Step three involves determining what is actually vibrating under the influence of these disturbances, and consequently causing the unwanted error in MAλ and MSDλ. To establish a relevant open-loop baseline, the existing wavelength stabilization control loop, using the stepper motor drive, was disabled during all testing presented here.

Figure 1 shows representative pulse by pulse wavelength error data during operation in burst mode, along with computed MAλ and MSDλ. Twenty-two 200-pulse bursts were acquired at this 1880 Hz repetition rate, each separated by 300 msec, for 26% duty-cycle. (Note that disabling the stepper motor loop also allows wavelength to drift, on a time scale much slower than any features seen here, so each burst was arbitrarily referenced to zero error at its final pulse.) Several features are evident in the raw wavelength data. There is a repeatable component with a fast transient at the beginning of the burst and a slower transient through the remainder of the burst. The fast transient impacts MSDλ in the first few 30-point windows, while the slow transient impacts MAλ. There is also a random component to the wavelength error, which does not affect MAλ, but contributes an 0.02 picometer RMS base level to MDSλ.

Vibration contributes to both the deterministic and the random components of wavelength error. To understand the deterministic component, it is important to remember that wavelength error is in effect a sampled data stream. The pulse train disturbance may excite mechanical or acoustic resonances with natural frequencies at or near the repetition rate, or its harmonics. If these resonances impact wavelength, it will only be observable at the time of a pulse. The resonant oscillations will be at frequencies of at least twice the Nyquist frequency (which = ½ the repetition rate, or effective sampling rate), and so will be aliased, appearing as non-oscillatory transients in wavelength.

The fast transient seen in Figure 1 causes the largest value of MSDλ, and is known to be due to chamber acoustics. This was validated in the present study by acquiring data similar to that in Figure 1 at a range of repetition rates from 1000 to 2500 Hz,

and plotting the worst-case MSDλ from each (Figure 2). Circles denote instances of worst-case MSDλ due to the fast initial transient, e.g. at most of the repetition rates considered. Frequencies of any acoustic modes in the chamber will scale according to the speed of sound, which is itself proportional to the square root of gas temperature. The associated peak frequencies of worst-case MSDλ will therefore increase with the square root of temperature if they are acoustically driven, and will not change with temperature otherwise. In Figure 2, two sets of data are presented, taken with chamber temperatures of 37°C (310K) and 58°C (331K). The 37°C data is plotted using a frequency vector scaled by 1.033 (the square root of the temperature ratio), which causes the major features to align with the higher-temperature data, exactly as would be expected of acoustically-induced error. It should be noted here that the testbed laser is within specified MSDλ limits, and well within them below the 2000 Hz specified maximum repetition rate.

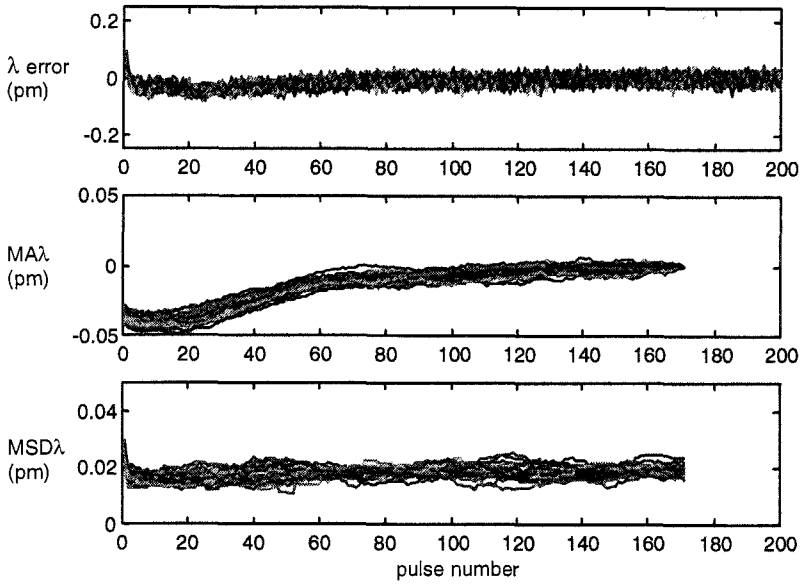

Figure 1: Representative wavelength error data, with computed moving average and moving standard deviation from the testbed laser.

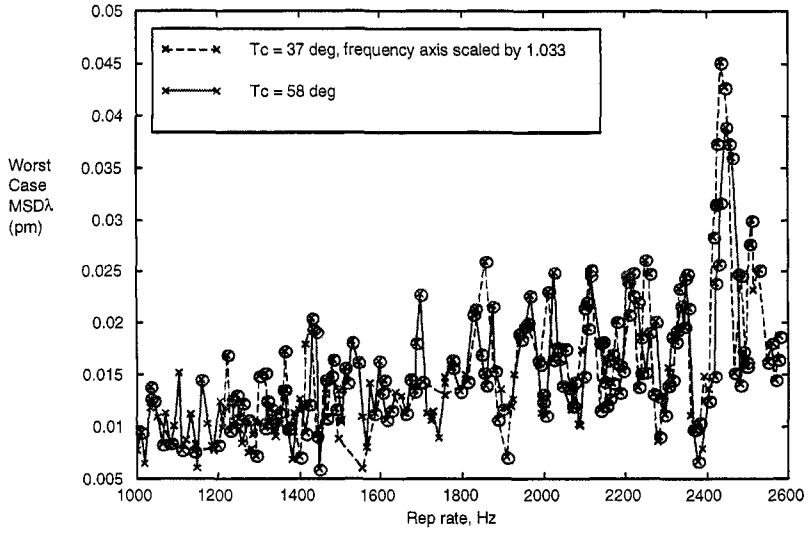

Figure 2: Worst-case burst-mode MSDλ as a function of repetition rate, with all wavelength control disabled, and all random components averaged out in post-processing: comparing two chamber temperatures.

The slow transient in wavelength error during a burst is likely also associated with aliased resonant responses, and though it does not impact worst-case MSDλ, it is the key source of MAλ error. Figure 3 illustrates an example repetition rate at which the amplitude of mechanical vibration, measured using a structural sensor, shows correlation with the slow transient behavior in wavelength error. In this case, a high-bandwidth sensor was used to measure the force was the PZT stack in the LNM. The PZT stack is in fact a transducer, not just a motor. It was not controlled during this measurement, so its sensing capability was useable. Similar correlations were seen at a few other repetition rates, using the force sensor as well as other diagnostic sensors. In general, however, mechanical vibrations were not seen to be a significant source of wavelength error, in the moving mean or moving standard deviation, at most repetition rates tested. Thus it can be inferred that the laser discharge is not a significant source of disturbance outside of the chamber acoustics.

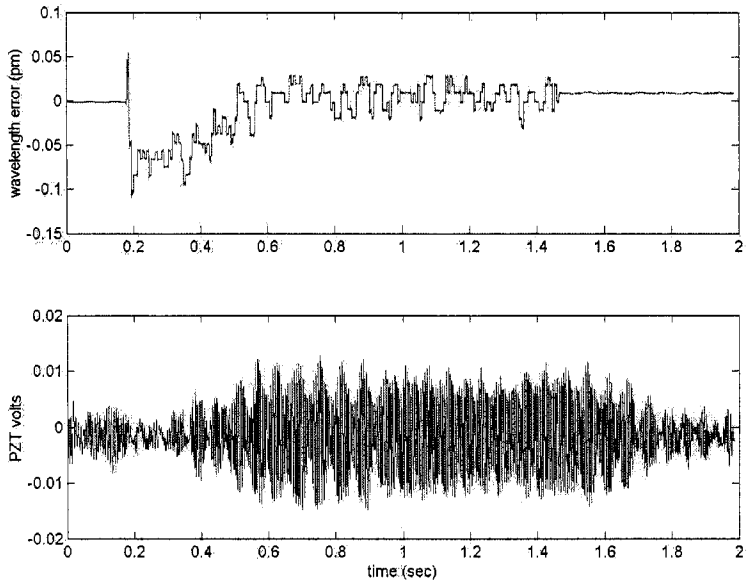

Figure 3: Correlation between slow transient wavelength error and amplitude of vibration as measured by the PZT stack as a sensor.

The random component of wavelength error is associated with frequencies that do not correspond to the pulse repetition rate, and therefore must be caused by another disturbance source. To identify the frequency content of the random error, autospectra of burst data were computed (Figure 4). Most of the spectral energy lies in three fairly narrow frequency bands, though aliasing causes the two higher-frequency bands to apparently shift in frequency at different repetition rates[1]. A spectral peak at frequency f in the wavelength error at repetition rate f_R may in fact be due to some underlying oscillation at any one of the frequencies in the set

$$\{Nf_R - f, Nf_R + f\}, \quad N = 1,2,3,\cdots. \tag{1}$$

True frequencies were determined by over-plotting spectra of data acquired at seven randomly selected repetition rates, and searching for common values in the sets of possibilities. Major frequency components were thus found to lie at 178 Hz, 2680 Hz, and in a band from 1100-1200 Hz containing a cluster of at least three constituent peaks and roughly 50% of the error spectral energy. The error associated with the slow and fast deterministic transients appears at 0 Hz in these plots, and its spectral energy is not included in the calculation.

The spectral peaks in Figure 4 were shown to be caused by the circulating fan in the chamber. This was determined by monitoring the wavelength error and several high-bandwidth structural sensors simultaneously, including the force sensor discussed above, with a spectrum analyzer. Key peaks in the structural sensors spectra were identified which corresponded to the peaks in the wavelength spectrum. These key peaks were seen to disappear with the fan turned off, and reappear with it turned on.

The frequency components in the wavelength error spectrum could come from two sources: forced response or modal response. Forced response in this case refers to motion of key components excited away from any structural resonances by the fans, while modal response implies excitation of a resonant structural mode, with the associated dynamic amplification of the underlying disturbance. It is possible to change fan speed in the ELS-6000, so we did (Figure 5). The major peaks

maintain a common frequency, and vary only in amplitude, suggesting modal response to the moving harmonics in the underlying fan disturbance spectrum.

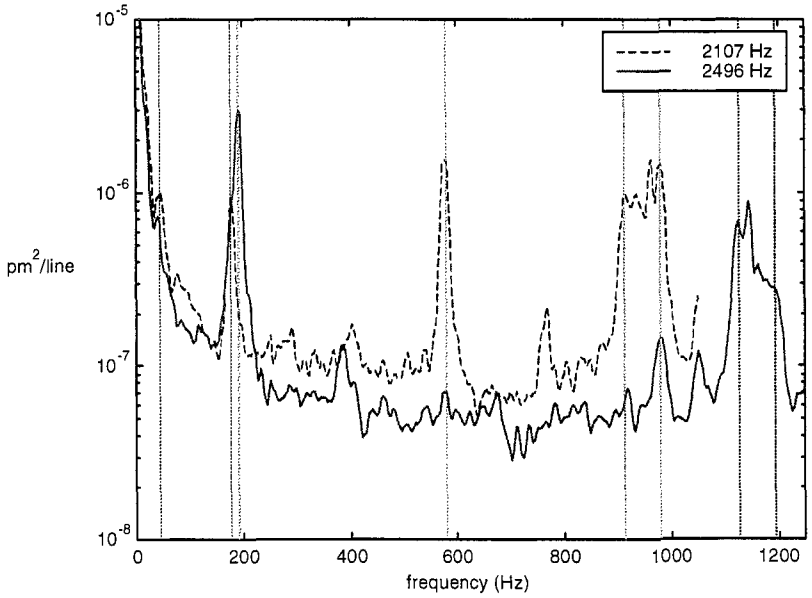

Figure 4: Autospectra of center wavelength error at two repetition rates.

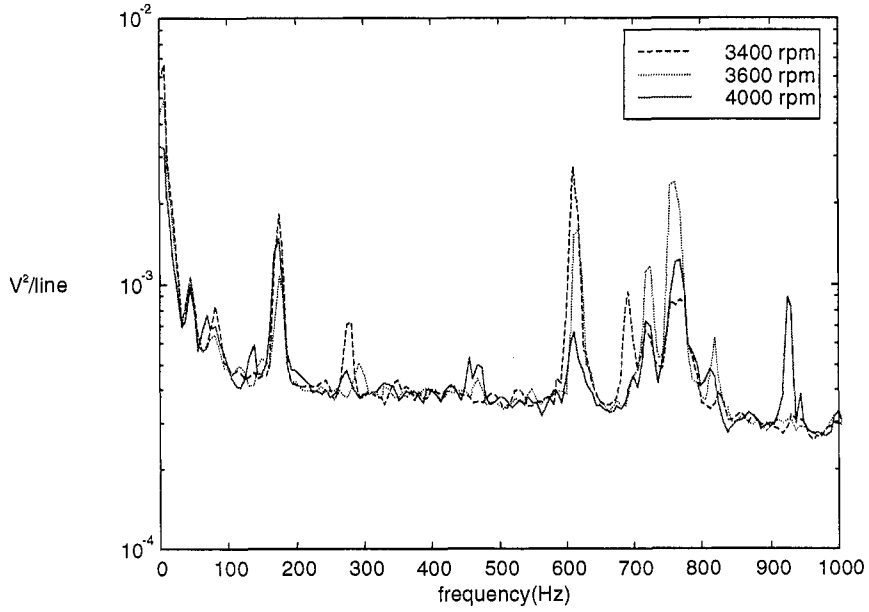

Figure 5: Autospectra of center wavelength error at 2 kHz repetition rates and multiple fan speeds.

With the performance metrics characterized, and the disturbance sources behind the error components identified, attention was next devoted to determining the structural mode shapes associated with those error components. Generally speaking, a mode shape describes the motion of all points on a structure, including all major components, at a particular resonant frequency. (This definition is approximate, and does not necessarily apply to highly damped modes or modes closely spaced in frequency, and therefore dynamically coupled.) Modal testing[2] was performed using an impact hammer, instrumented with a force sensor measure the impact force pulse, and a set of acceleration sensors at strategic locations on the laser. Transfer functions between input force and acceleration (also known as frequency response functions) were computed for a number of different impact locations. The resulting data, along with geometric information about the laser frame structure and impact locations, was fed into a commercially available mode shape visualization package. A typical mode shape is

shown in Figure 6. This global mode, at 1190 Hz, includes rigid body and flexible motion of the LNM, to the right, as well as bending deformation of the three support rods. The chamber, not shown, is mounted in the area of the three rods.

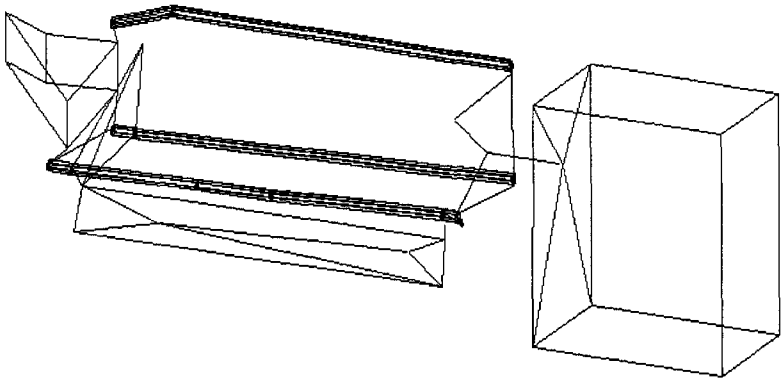

Figure 6: Experimentally-derived mode shape of 1190 Hz mode on testbed laser.

Another key mode in the 1100—1200 Hz cluster was found not by the modal test, which focused only on the exterior of the LNM and the support structure, but by driving the PZT stack with band-limited white noise through a power amplifier, and measuring the acceleration of various points on the steering mirror in the LNM. This mode principally involves flexible deformation of the mirror and its mount, but the components of its drive train and the surrounding LNM housing structure also participate to some degree. This mode is physically localized to the mirror assembly, but it is moderately dynamically coupled to the surrounding modes in the cluster. All of those modes are therefore controllable from the PZT stack.

4. WAVELENGTH STABILITY ENHANCEMENT

Three key features of the wavelength error have been identified to this point. Each has a particular set of applicable and/or effective mitigation strategies. The fast transient, associated with acoustics, can be dealt with by passive mitigation techniques internal to the chamber, which will not be discussed here. The slow transient, regardless of its cause, can be dealt with by traditional servo control methods, provided a fast enough actuator for the beam steering mirror and a fast enough measurement of the wavelength at every pulse. The random component can be addressed on a mode-by-mode basis with a number of traditional passive and novel active control strategies. The steering mirror mode in the 1100—1200 Hz cluster is a good candidate for active vibration control, as redesign for stiffening has already been incorporated, and passive damping materials are not permitted inside the LNM due to degradation by the scattered DUV light, and the consequent contamination of the optics.

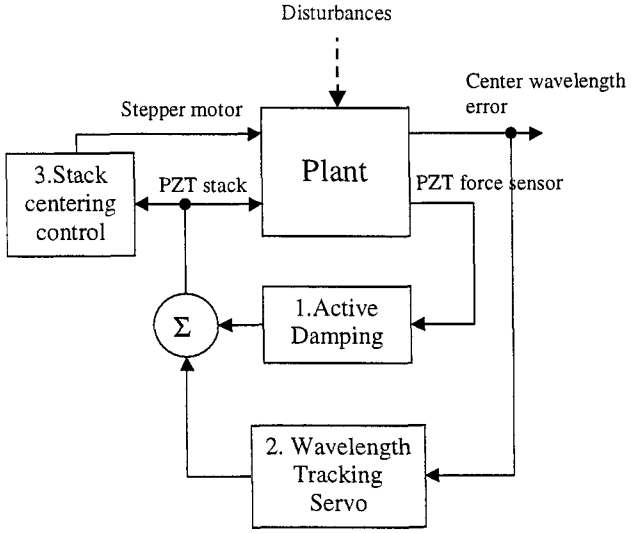

Figure 7: Functional block diagram of a candidate wavelength control system architecture.

Figure 7 shows a candidate active control architecture for wavelength stabilization. Block 2 is the servo described above, in which the wavelength error data is fed back to the PZT stack via a traditional proportional-plus-integral-plus-derivative (PID) algorithm. This type of control is well-understood[3], straightforward to design, and effective at controlling error in a bandwidth well below the first resonant mode in the system. In the present case, the frequency content of the slow transient lies below 100 Hz, while the first resonance in the plant transfer function (the frequency response of the wavelength error to PZT stack input) is above 1 kHz. The details of this control will not be discussed here. It has been implemented and tested at Cymer, and shown to be effective at controlling MAλ error, which is strongly dependent on the slow transient. In this new servo architecture, the existing stepper motor (block 3) assumes the new role of de-saturating the PZT stack when its mean control voltage strays too far toward its limits in response to, e.g., slow thermal drift.

The prime focus of this study was reduction in the portion of MSDλ error associated with random vibrations. This component of the error has not been addressed to date, but contributes significantly to the worst-case value at all repetition rates, as illustrated by Figure 8. The quantity plotted here as a dashed line is the same as in Figure 2: the worst-case value of MSDλ at each repetition rate, measured over a number of 200-pulse bursts. The second, solid trace is the worst-case MSD in a hypothetical system with no random component. This was calculated by averaging all bursts of wavelength error data at each repetition rate, which has the effect of correlating out the random component and leaving the deterministic component (the fast and slow transients). The fast transient is the only remaining feature with significant contribution to MSDλ. Regardless of the steps taken to mitigate the fast transient (again, none were implemented on the testbed laser, as none were needed to meet current specifications), removing the random error reduces MSDλ by about 0.01pm at all repetition rates. A combination of acoustic mitigation and vibration control could enable future generation lasers to meet specifications up to five times tighter than the current 0.05 pm.

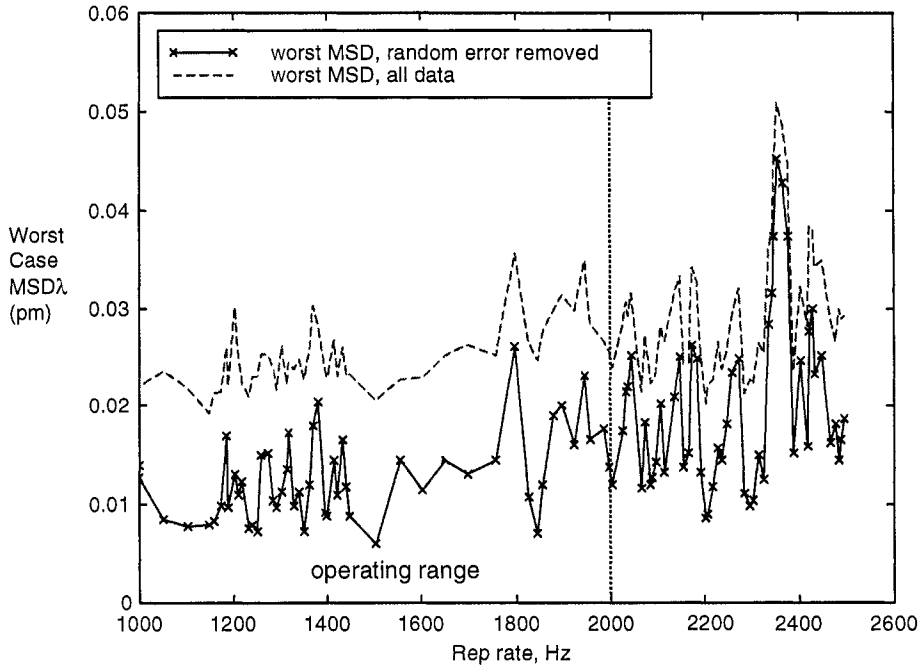

Figure 8: Worst-case MSDλ in the theroetical limit with all random error removed, with actual data for comparison.

The control architecture of Figure 7 allows the random component of error to be addressed in two ways. Active damping of modes which are controllable from the PZT stack is one possibility (block 1). A second possibility is enhancement of the wavelength error servo algorithm (block 2) using modern control design techniques.

Active damping control is a robust and effective means of minimizing vibrations due to structural modes with light inherent damping. Unlike servo control, which applies large gains at low frequency to achieve tracking or set point accuracy, active damping of lightly damped modes involves applying relatively small feedback gains, with the proper phasing, in the frequency region of resonant response[4,5]. When properly designed, active damping systems are robust to uncertainties in

resonant frequencies and amplitudes, both in terms of performance and stability. Keys to successful active damping design include proper choice and location of sensors, actuators, along with appropriate selection of the feedback control filter. Sensor and actuators should be co-located and dual. Co-location ensures robustness[6,7]. Duality, implying that the product of sensed and actuated quantities is work (or, strictly speaking, power), ensures the proper combination of controllability of target modes from the actuator, and observability from the sensor.

Diagnostic testing indicated that several of the modes contributing to the random component of wavelength error are controllable from the PZT stack in the LNM. This was demonstrated by measuring the transfer function from the PZT stack to the wavelength error under swept sine excitation, and also by measuring the transfer function from PZT stack to acceleration sensors on the steering mirror under broadband random excitation. The PZT stack has a high inherent stiffness (mechanical impedance) relative to the sprung steering mirror assembly (Figure 8), and therefore acts as a position actuator under applied voltage. The proper dual quantity is therefore co-located force[8], sensing of which was achieved by inserting a thin PZT wafer at the driving point. If the PZT stack were relatively soft compared to the driving-point impedance, a position sensor would be more appropriate. In intermediate cases, a combination of the two would be ideal for active damping[9].

The PZT sensor sketched in Figure 8 was custom-designed for this study, to meet sensitivity requirements imposed by the small vibratory forces in the PZT stack drive mechanism. The small vibratory force is consistent with the small disturbance levels and displacements present in most semiconductor manufacturing equipment designed to realize on-wafer critical dimensions of 180 nm and below. In the small-signal regime, PZT material has V/N sensitivity proportional to $g_{33}t$, where g_{33} is a piezoelectric material constant and t is the PZT thickness. ACX manufactured the force sensor using QuickPack® packaging technology, which isolates the PZT from the environment and mechanically robustifies the otherwise brittle ceramic material, and also provides easy electrical connections to the PZT wafer's electrodes. The device used here was based on type 5A PZT material.

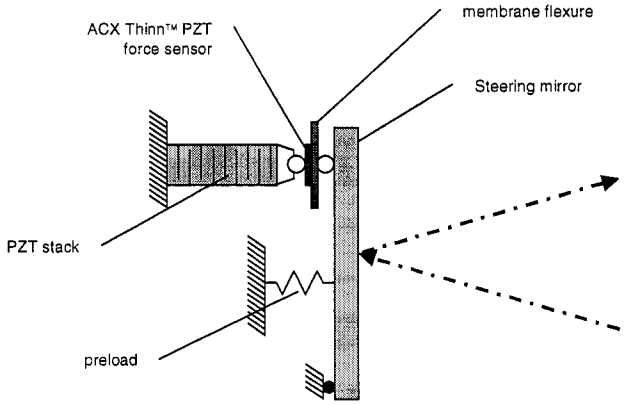

Figure 9: Mechanical arrangement of actuator, sensor, and steering mirror used in active damping loop.

Several types of control filter are applicable to active damping architectures. In the present case, with a single actuator/sensor pair and a few well-spaced (in frequency) modes to be controlled, narrowband filters provide the correct combination of gain and phase at the natural frequency of interest, while adding little or no feedback gain elsewhere, enhancing stability. Such a control approach has been called Positive Position Feedback (PPF)[10], though it applies equally well to the adjoint problem of force feedback to a position actuator. Control design was accomplished here first by creating a state-space plant model, G, from transfer function data using the Smart ID system identification software package. The filter, K, was designed by selecting the parameters of the continuous second order system (shown here in the Laplace domain)

$$K(s) = a\frac{s - z}{s^2 + 2\zeta\omega s + \omega^2}, . \tag{2}$$

to achieve 0° loop phase (phase of GK), and loop gain of some value > 1 at the modal frequency. Here s is the Laplace variable, z is a real zero used to tune phase, ζ is the filter damping ratio used to select the bandwidth of the damping, ω is the filter natural frequency, and a is the gain factor. This filter was discretised using the Tustin transform with frequency

prewarping, and closed loop performance was simulated, using the ID system model from data acquired at 2100 Hz repetition rate (Figure 10). The active damping control was predicted to reduce RMS wavelength error by 0.006 pm.

The second approach to reducing MSDλ involves enhancing the wavelength servo algorithm in block 2 of Figure 7 using modern model-based optimal control design methods[11]. The discrete-time plant model developed here (where in this case the plant has the PZT stack as input and the wavelength error as output, while the active damping loop is closed) was used to design a Linear Quadratic Gaussian (LQG) compensator. Proper weighting of the LQG problem resulted in a compensator which applied gain over very narrow ranges, corresponding to the spectral peaks not addressed by the damping. Unlike active damping, this type of feedback does not actually attenuate the physical response of the problem modes. Instead, it effectively extends the bandwidth of the servo such that the high frequency components are tracked, and their effects thus rejected from the wavelength error. This type of compensation can be very effective, and is theoretically interesting; however in the present case it was shown to reduce RMS wavelength error by only an additional 0.001 pm over the active damping – primarily because the spectral peaks rejected contained only a small part of the total error energy.

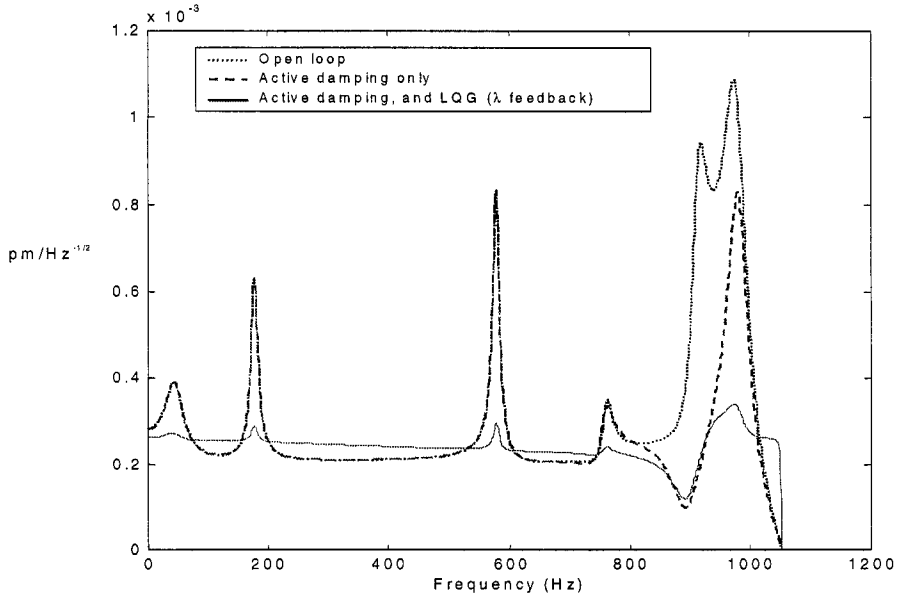

Figure 10: Open and closed-loop wavelength error autospectra at 2100 Hz repetition rate, from ID of data and simulation of controls.

5. BREADBOARD TESTING

With the PZT stack and PZT force sensor in place in the testbed laser, it was a simple matter to implement the (more effective) active damping controller designed above. The ACX Modular Control Platform (MCP) was used in these experiments. The MCP is based around a single-board computer (SBC) using a Texas Instruments C32 digital signal processor (DSP). This processor is able to implement real-time control at rates up to 50 kHz, depending upon the size of the filter and the desired control bandwidth. Here, a 20 kHz rate was used. The MCP includes a signal conditioning card designed for PZT sensors (force or strain), as well as amplifier cards designed to drive PZT actuators. (Other sensors and actuators an be accommodated with other cards.) The MCP uses a modular software architecture which allows rapid prototyping of controllers via online system ID routines and easy filter downloads from the Matlab design environment.

Performance data is shown in Figures 11 and 12. Figure 11 shows the wavelength error autospectrum (without the pm/V scale factor included) acquired at 2100 Hz repetition rate with the active damping loop open and closed. In both cases the ELS-6000 production-version wavelength servo (stepper motor only) was disabled. Performance achieved exceeded the analytical predictions, with a 0.008 pm RMS reduction demonstrated. Comparing Figures 11 and 10, it is evident that the ID model did not accurately capture the dynamic coupling between all of the modes in the 1100-1200 Hz cluster (all aliased below the 1050 Hz Nyquist frequency).

Figure 12 shows MSDλ data computed from a number of bursts at 2100 Hz repetition rate. In this case, the worst MSDλ improved dramatically by 0.018 pm, from 0.048 pm to 0.030 pm. However, it should be noted that some of this reduction is due to an abnormally large open-loop random error component. Several months had passed between collection of the

original data shown in Figures 1 and 2, and the closed-loop testing discussed in this section. In the interim, one of the bearings supporting the chamber circulation fan had exceeded its normal maintenance interval. The bearing wear caused the fan disturbance to be amplified. However, in a nominally-performing laser, it is still reasonable to expect a reduction of up to 33% in the worst-case MSDλ at repetition rates not normally subject to large amplitude fast acoustical transients.

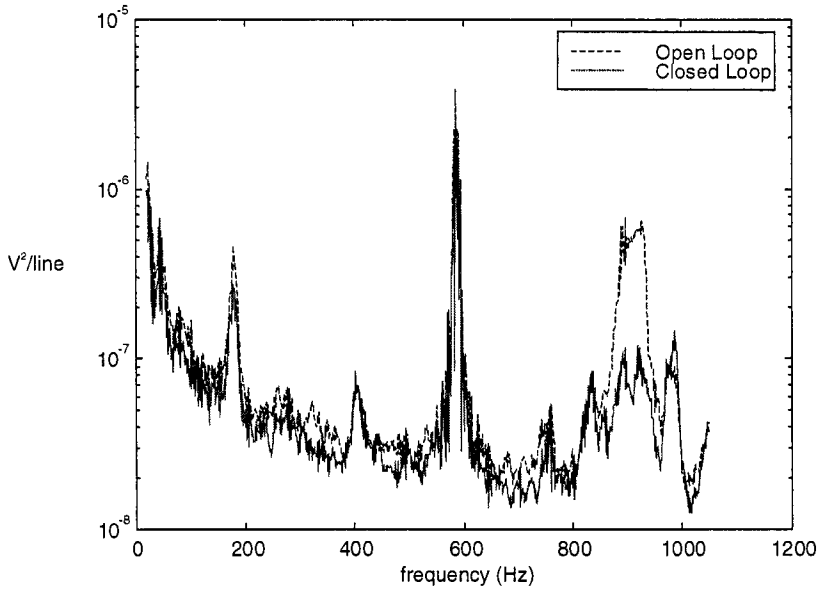

Figure 11: Open and closed loop (active damping) autospectrum data at 2100 Hz repetition rate.

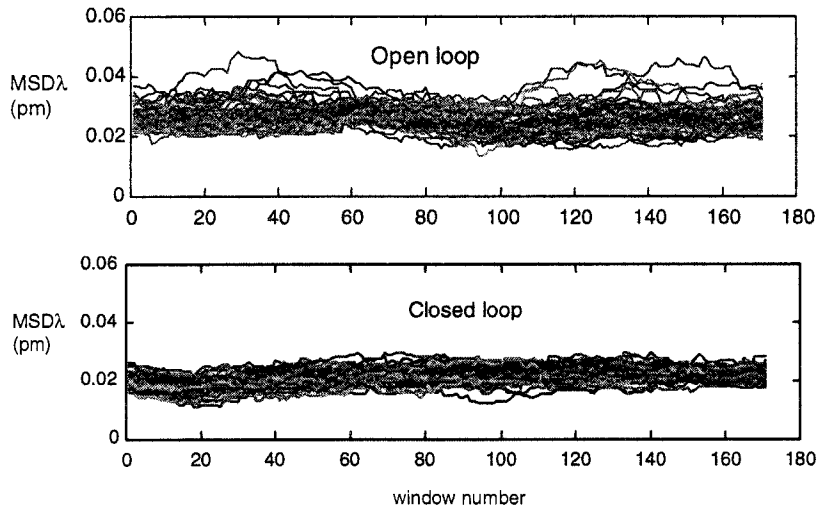

Figure 12: Open and closed loop (active damping) MSDλ data at 2100 Hz repetition rate,.

6. CONCLUSIONS

Wavelength stabilization through active control is a viable and effective path to meeting the requirements expected to be imposed on future generation excimer lasers used in semiconductor processing. Both moving-window average and moving-window standard deviation of wavelength error, relative to the desired set-point, are addressable given the proper feedback sensor and control law. Current state-of-the-art in industrial controls may be sufficient to address the relatively slow component of error captured by the moving average. This type of servo control requires an accurate measurement of the wavelength for each pulse, delivered with a minimum of measurement and computation delay. The control algorithm is as simple as a few lines of code. Errors due to higher-frequency disturbances, and the associated acoustical and mechanical resonances they induce into the laser systems, require a new type of control. The modern control theory on which this new

design is based is fairly complex, but the resulting control for this particular problem can also be fairly simple in form, and therefore robust and easy to implement. Based on the analytical and experimental results presented here, application of these classical and modern control techniques could allow future generation lasers to achieve as much as a fivefold tightening of stability specifications.

7. ACKNOWLEDGEMENTS

The authors wish to thank Dr. David Warkentin, and Mr. Marco Giovanardi at ACX for their support in the experimentation and analysis efforts associated with this study. The authors also wish to thank Dr. Igor Fomenkov at Cymer, for discussions which helped to clarify the link between optical component motion and wavelength error, and Mr. David Myers at Cymer for his support of this project.

8. REFERENCES

[1] Franklin, G. F., and Powell, J. D., *Digital Control of Dynamic Systems*, Chapter 4, Addison Wesley, Reading, MA, 1980.
[2] Ewins, D. J., *Modal Testing: Theory and Practice*, Research Studies Press LTD., Taunton, Somerset, England, 1984.
[3] D'Azzo, J. J., and Houpis, C. H., *Feedback Control System Analysis and Synthesis*, 2d Edition, McGraw-Hill, New York, 1966.
[4] Aubrun, J.-N., "Theory of the Control of Structures by Low-Authority Controllers," *AIAA Journal of Guidance & Control*, **Vol. 3**, No. 5, pp. 444—451, Sept-Oct 1980.
[5] Balas, M. J., "Direct Velocity Feedback Control of Large Space Structures," *AIAA Journal of Guidance & Control*, **Vol. 2**, No. 3, pp. 252—253, May-June, 1979.
[6] Joshi, S. M., "Robustness Properties of Collocated Controllers for Flexible Spacecraft," *AIAA Journal of Guidance, Control & Dynamics*, **Vol. 9**, No. 1, pp. 85—91, 1986.
[7] Spangler, R., and Hall, S. R., "Broadband Active Structural Damping Using Positive Real Compensation and Piezoelectric Simultaneous Sensing and Actuation," *Journal of Smart Materials and Structures*, **Vol. 3**, No. 4, December 1994.
[8] Premont, A., Dufour, J.-P., and Malèkian, "Active Damping by a Local Force Feedback with Piezoelectric Actuators," *AIAA Journal of Guidance, Control, and Dynamics*, **Vol. 15**, No. 2, pp. 390—395, 1992.
[9] Chen, G.-S., Lurie, B. , "Active Member Bridge Feedback Control for Damping Augmentation," *AIAA Journal of Guidance, Control & Dynamics*, **Vol. 15**, No. 5, pp. 1155—1160, 1992.
[10] Fanson, J. L., and Caughey, T. K., "Positive Position Feedback Control for Large Space Structures," *AIAA Journal*, **Vol. 28**, ,pp. 717—724, 1990.
[11] Lublin, L., Grocott, S., and Athans, M., "H_2 (LQG) and H_∞ Control," in *The Control Handbook*, William S. Levine, Editor, pp. 651—662, CRC Press, 1996.